

Quantum oscillations in a topological insulator $\text{Bi}_{1-x}\text{Sb}_x$

A. A. Taskin and Yoichi Ando

Institute of Scientific and Industrial Research, Osaka University, Osaka 567-0047, Japan

We have studied transport and magnetic properties of $\text{Bi}_{1-x}\text{Sb}_x$, which is believed to be a topological insulator — a new state of matter where an insulating bulk supports an intrinsically metallic surface. In nominally insulating $\text{Bi}_{0.91}\text{Sb}_{0.09}$ crystals, we observed strong quantum oscillations of the magnetization and the resistivity originating from a Fermi surface which has a clear two-dimensional character. In addition, a three-dimensional Fermi surface is found to coexist, which is possibly due to an unusual coupling of the bulk to the surface. This finding demonstrates that quantum oscillations can be a powerful tool to directly probe the novel electronic states in topological insulators.

PACS numbers: 71.18.+y, 71.70.Di, 73.43.-f, 85.75.-d

Bi and $\text{Bi}_{1-x}\text{Sb}_x$ alloys have been “gold mines” of modern solid-state physics for over seven decades [1, 2, 3, 4, 5, 6, 7]. The discovery of quantum oscillations itself has been made on pure Bi as long ago as 1930. The anomalously large diamagnetism in Bi was a fundamentally important problem [1] and prompted the application of the Dirac theory to solid states [1, 2] in the 1960’s. Also, $\text{Bi}_{1-x}\text{Sb}_x$ is known as one of the best thermoelectric materials [3] and consequently has been studied in great detail. As a result, Bi and $\text{Bi}_{1-x}\text{Sb}_x$ have been thought to be very well understood. Yet, a new twist came recently [8, 9, 10, 11, 12, 13, 14, 15, 16, 17, 18, 19, 20] from new ideas about topological phases in condensed matter [8, 9, 10, 11, 12, 13, 14]; namely, it has been realized that $\text{Bi}_{1-x}\text{Sb}_x$ in the insulating regime ($0.07 < x < 0.22$) is a “topological insulator” (TI) that belongs to a non-trivial Z_2 topological class [9]. Since the vacuum belongs to a trivial topological class, a smooth transition from a TI to the vacuum is possible only by closing the energy gap along the way, making the surface of a TI to be intrinsically conducting. Intriguingly, those metallic surface states are expected to be spin-filtered, obey Dirac-like energy dispersion, and be topologically protected [8, 9, 10, 11].

In the past, a metallic behavior has always been observed at low temperature in $\text{Bi}_{1-x}\text{Sb}_x$; namely, its resistivity has never presented a true divergence in the zero-temperature limit, even in the insulating doping range where a bulk energy gap opens [3]. The origin of this metallic state at low temperature has never been fully understood and was mainly attributed to imperfections of measured crystals, in particular, to the formation of an impurity band within the bulk energy gap. On the other hand, recent angle-resolved photoemission spectroscopy (ARPES) studies on its cleaved (111) trigonal surface have revealed that the energy dispersions of the surface states possess the distinctive character to qualify this material as a topological insulator [16, 17, 18, 19, 20], so it is natural to ask whether the low-temperature metallic behavior of “insulating” $\text{Bi}_{1-x}\text{Sb}_x$ has anything to do with the topological surface state. In the present work, to directly address this question, we measure quantum oscil-

lations (QOs) in nominally insulating $\text{Bi}_{0.91}\text{Sb}_{0.09}$ crystal to differentiate a coherent electronic transport on a fully developed Fermi surface (FS) from an incoherent transport within an impurity band.

$\text{Bi}_{1-x}\text{Sb}_x$ crystals were grown from a stoichiometric mixture of 99.9999% purity Bi and Sb elements by a zone melting method. The homogenization of $\text{Bi}_{1-x}\text{Sb}_x$ microstructure was achieved by multiple (~ 100 times) re-melting of the boule. The last run for each growth was done at a very low rate (≤ 0.2 mm/h) to avoid constitutional supercooling and the resulting segregation of the solid solution. All grown crystals were easily cleaved along the (111) plane, revealing flat, shiny surfaces. To prepare samples suitable for transport and magnetic measurements, crystals were aligned using the X-ray Laue analysis and cut along the principal axes. The actual composition of grown crystals and their purity were checked by the inductively-coupled-plasma atomic-emission spectroscopy (ICP-AES) analysis, which confirmed that the composition of grown $\text{Bi}_{1-x}\text{Sb}_x$ was close to the nominal value and that the concentration of any impurity atoms was less than the sensitivity threshold ($\sim 10^{21} \text{ m}^{-3}$). The resistivity was measured by a standard four-probe method on a rectangular sample with the size of approximately $1.5 \times 0.2 \times 0.1 \text{ mm}^3$. The electric current was directed along the C_3 axis, and the magnetic field was applied along the C_2 axis. For the de Haas-van Alphen (dHvA) measurements, a sample of approximately cubic shape and the mass of ~ 80 mg was cut along the principal crystallographic axes from the same $\text{Bi}_{0.91}\text{Sb}_{0.09}$ crystal as was used for the resistivity measurements. The dc magnetization M was measured in magnetic fields up to 1 T at fixed temperatures in the range from 2 to 40 K using a commercial Quantum Design SQUID magnetometer. Quasi-equilibrium measurement conditions allowed us to observe even a weak modulation of the magnetization in fields as low as 0.08 T.

The temperature dependences of the resistivity, $\rho_{xx}(T)$, for three high-quality $\text{Bi}_{1-x}\text{Sb}_x$ crystals with increasing Sb concentration, $x = 0.00, 0.06, \text{ and } 0.09$, are shown in Fig. 1(a). A qualitative change from a metallic behavior with positive slope $d\rho/dT > 0$ to an insulator-

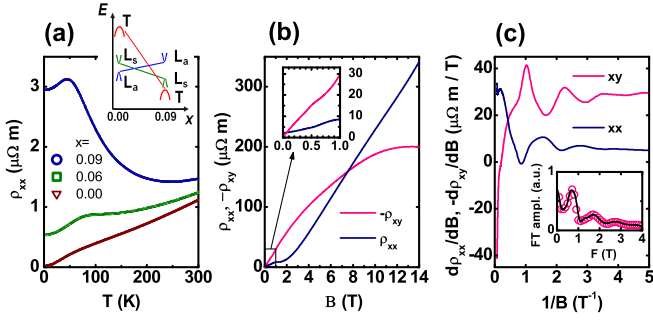


FIG. 1: (Color online) (a) Temperature dependences of ρ_{xx} for $x = 0.00, 0.06,$ and 0.09 . Inset shows a diagram of the evolution of the energy bands in $\text{Bi}_{1-x}\text{Sb}_x$ upon doping. (b) Magnetic-field dependences of ρ_{xx} and $-\rho_{xy}$ in $\text{Bi}_{0.91}\text{Sb}_{0.09}$ at 1.4 K. (c) Derivatives of $\rho_{xx}(B)$ and $-\rho_{xy}(B)$ vs. B^{-1} . Inset shows the FT spectrum of the $-\rho_{xy}$ oscillations.

like behavior is clearly seen between $x = 0.06$ and 0.09 . This indicates that, at $x = 0.09$, an energy gap for charge carriers fully opens, in agreement with recent ARPES measurements [18, 19, 20] as well as the well-established evolution of the energy bands in $\text{Bi}_{1-x}\text{Sb}_x$ upon doping [3, 5]. The change from the semimetal nature in pure Bi ($x = 0.00$), resulting from an overlap of the valence and conduction bands at different points in the Brillouin zone (BZ), to the bulk-insulator nature at $x = 0.09$ with a direct gap at the zone boundary is schematically depicted in the inset of Fig. 1(a). Despite the upturn in the resistivity below 200 K, the sample with $x = 0.09$ shows a metallic behavior below 40 K, even though the resistivity value is about 100 times larger than in pure Bi in the zero-temperature limit.

Figure 1(b) shows that both ρ_{xx} and ρ_{xy} of the $x = 0.09$ sample change strongly with the magnetic field B at 1.4 K. The $\rho_{xx}(B)$ shows an almost linear increase above ~ 2 T and, at 14 T, it is ~ 170 times larger than at 0 T. The $\rho_{xy}(B)$, on the other hand, is almost linear at low fields and shows a saturation around 14 T. The negative slope of $\rho_{xy}(B)$ at $B = 0$ T suggests that the main carriers in the sample are electrons [note that $-\rho_{xy}(B)$ is plotted in Fig. 1(b)]. The Hall coefficient R_H estimated from the slope is $-3.5 \times 10^{-5} \text{ m}^3/\text{C}$, implying that the concentration of electrons in the sample is of the order of $|1/eR_H| \approx 1.8 \times 10^{23} \text{ m}^{-3}$. At low fields, both $\rho_{xx}(B)$ and $\rho_{xy}(B)$ show a weak modulation in the magnetic field (more clearly seen in the inset). Their derivatives with respect to B plotted vs. $1/B$ [Fig. 1(c)] reveal clear Shubnikov-de Haas (SdH) oscillations in magnetic fields below ~ 2 T. The Fourier transform (FT) of $d\rho_{xy}/dB$ [Fig. 1(c) inset] yields the power spectrum with the leading frequency of 0.67 T. Such an observation of QOs in a nominally insulating material is surprising, and we elucidate their origin in the following.

The dHvA effect, which we also observe in our $\text{Bi}_{0.91}\text{Sb}_{0.09}$ crystal, is another way of probing the Fermi

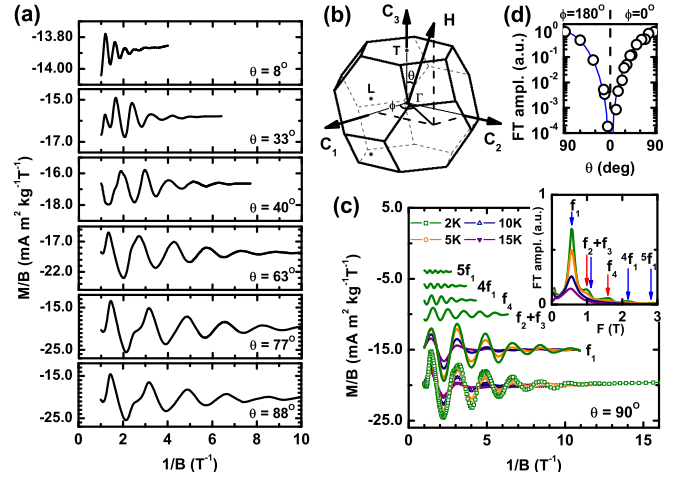


FIG. 2: (Color online) (a) Example of the angular dependence of the dHvA oscillations in $\text{Bi}_{0.91}\text{Sb}_{0.09}$ at 2 K for magnetic fields in the binary plane (*i.e.*, θ is varied, while $\phi = 0^\circ$ is fixed). (b) Schematic picture of the bulk Brillouin zone of $\text{Bi}_{1-x}\text{Sb}_x$ and the geometry of the experiment. (c) Example of the decomposition of the raw M/B data (shown by symbols at the bottom) into a set of oscillatory parts (shown by straight lines); inset shows the FT spectra at 2, 5, 10, and 15 K for $\theta = 90^\circ$ and $\phi = 180^\circ$. (d) θ dependence of the FT amplitude of the main peak f_1 within the binary plane.

surface. This effect is manifested in magnetization which is a very straightforward thermodynamic property. An example of oscillations of the magnetic susceptibility M/B measured at 2 K with the magnetic field direction lying in the binary plane (perpendicular to the C_2 axis) at different angles θ is shown in Fig. 2(a), where a complex structure of the oscillations as well as changes in their amplitudes and periods are clearly seen. Shown in Fig. 2(b) is a schematic representation of the BZ, three main axes, positions of high symmetry points, and geometry of the present experiment. The Fourier analysis is applied to all measured data to obtain quantitative information, and Fig. 2(c) shows, as an example, the decomposition of magnetic oscillations into a set of constituents for $B \parallel C_1$ axis. The experimental data are shown at the bottom by symbols. The inset of Fig. 2(c) displays the FT spectra for four measured temperatures; several frequencies can be readily distinguished, and up to the fifth harmonic of the lowest frequency f_1 can be identified at 2 K, indicating a high degree of coherence [21]. The angular dependence of the FT amplitude of the main peak f_1 for magnetic fields in the binary plane is shown in Fig. 2(d). This amplitude exhibits a very sharp decrease by as much as four orders of magnitude when the magnetic-field direction approaches the bisectrix plane (perpendicular to the C_1 axis), as if carriers cannot move perpendicular to this plane to make Larmor orbit. This angular dependence is the first indication of a two-dimensional (2D) nature of the corresponding FS.

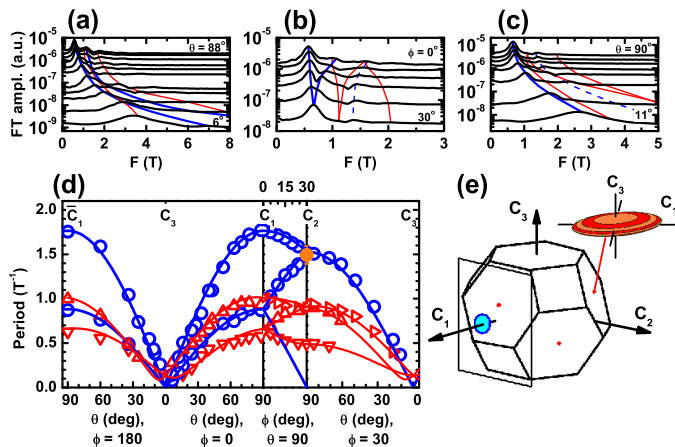


FIG. 3: (Color online) (a)–(c) Evolution of the FT components of the dHvA oscillations upon rotating the magnetic field within the (a) binary, (b) trigonal, and (c) bisectrix planes. The lines are guides to the eye, and the dashed lines denote those peaks that are not independent but come from higher harmonics or interference of independent frequencies. (d) Angular dependences of P ($= 1/F$) within the three main planes; experimental data, corresponding to the peaks in (a)–(c), are shown by symbols. Thick (blue) and thin (red) solid lines are the fits using the model considering the 2D and 3D Fermi surfaces, respectively (see text). (e) Schematic picture of the surface and bulk FSs and their positions in the BZ.

Since the frequencies of QOs, F , are directly related to the Fermi-surface cross sections via the Onsager relation $F = (\hbar c/2\pi e)A$, where A is the area of an extremal cyclotron orbit, the shape and size of the FS can be obtained from the angular dependences of F measured within the three main crystallographic planes. To separate the FT peaks associated with different Fermi surfaces, the angle-dependent FT spectra in the binary, trigonal, and bisectrix planes (which are perpendicular to the C_2 , C_3 , and C_1 axes, respectively) has been mapped [Figs. 3(a)–3(c)]. By following the change in position of individual peaks in the spectra with changing angle, as shown in Figs. 3(a)–3(c) by lines, it is easy to sort out the evolution of each peak, which allows us to plot the angular dependences of all periods $P = 1/F$ of the dHvA oscillations within the three main planes, as shown in Fig. 3(d) by symbols. The period of the SdH oscillations [Fig. 1(c)] is also shown by a filled circle in Fig. 3(d). The branches in Fig. 3(d) are separated into two sets: In the binary plane ($\bar{C}_1 - C_3 - C_1$), two branches (shown by open circles) are symmetrical with respect to the positive (C_1) and negative (\bar{C}_1) axis direction and have a minimum (in fact, approaching zero) at exactly $\theta = 0^\circ$, while the other two branches (shown by open triangles) are slightly shifted with respect to $\theta = 0^\circ$.

Taking into account all three planes, the angular dependences of the observed periods point to a coexistence of 2D and 3D Fermi surfaces: The 2D one is a circle of

radius $k_F = 4.15 \times 10^7 \text{ m}^{-1}$ in the surface BZ of the bisectrix ($2\bar{1}\bar{1}$) surface, which is perpendicular to the C_1 axis, and there are six of them by symmetry. The size of this circle corresponds to the surface charge-carrier concentration $n_s = k_F^2/4\pi = 1.4 \times 10^{14} \text{ m}^{-2}$, if the surface state is spin-filtered; it will be twice as large, if the state is not spin-filtered. Branches calculated in this model are shown in Fig. 3(d) by thick (blue) solid lines, which match the data almost completely. The 3D FS is a set of three ellipsoids, located at the L points of the BZ with semi-axes $a = 2.7 \times 10^8 \text{ m}^{-1}$, $b = 1.3 \times 10^8 \text{ m}^{-1}$, and $c = 2.3 \times 10^7 \text{ m}^{-1}$ that are approximately along C_1 , C_2 , and C_3 , respectively; to be precise, the ellipsoids are tilted by $\sim +6^\circ$ in the binary planes [see Fig. 3(e)]. The size of each ellipsoid corresponds to the bulk charge carrier concentration of $abc/3\pi^2 = 2.7 \times 10^{22} \text{ m}^{-3}$. In total, three ellipsoids give $\sim 8.1 \times 10^{22} \text{ m}^{-3}$. Calculated branches for those 3D states are shown in Fig. 3(d) by thin (red) solid lines, which, again, match the data very well. The shapes of the 2D and 3D FSs are schematically shown in Fig. 3(e).

An important parameter that can be extracted from the dHvA oscillations is the cyclotron mass m_c . The temperature dependences of the oscillation amplitude for different angle θ (with fixed $\phi = 0^\circ$) are shown in Fig. 4(a), where fittings of the data to the standard Lifshitz-Kosevich theory [22] are shown by solid lines [23]. This analysis gives the angular dependence of m_c associated with the surface states as shown in Fig. 4(b). Two prominent features are readily recognized: First, the absolute value of m_c in the magnetic field perpendicular to the surface ($\theta = 90^\circ$) is extremely small, measuring only $0.0057m_e$ (m_e is the free electron mass), which is smaller than the cyclotron mass in pure Bi for any direction. Such a small m_c is the reason why it is possible to observe pronounced oscillations at relatively low magnetic fields. Second, $m_c(\theta)$ diverges at $\theta = 0^\circ$ and shows the $1/\sin\theta$ dependence that is characteristic of a 2D FS, giving unambiguous evidence for the 2D nature [24].

Once m_c is known, the scattering time τ is obtained by analyzing how M/B changes with B^{-1} at fixed temperatures. Figure 4(c) shows the Dingle plots [22], which yields the Dingle temperature T_D ($= \hbar/2\pi\tau k_B$), for the same field directions as in Fig. 4(a). All curves show linear slopes and for all angles the same T_D of 6.7 K (which corresponds to $\tau \approx 1.8 \times 10^{-13} \text{ s}$) is obtained. This is surprisingly low effective temperature for an alloy with this doping concentration [22]. Since the Fermi velocity v_F can be approximated by $v_F = \hbar k_F/m_c \approx 8.5 \times 10^5 \text{ m/s}$, the mean free path ℓ on the surface is estimated as $\ell = v_F\tau \approx 150 \text{ nm}$, which is comparable to the de Broglie wave length $\lambda = 2\pi/k_F \approx 150 \text{ nm}$ for the 2D FS. In passing, we note that our samples have a rectangular shape and four of the surfaces were cut along the C_3 axis with a wire saw; hence, those four surfaces are actually a collection of locally-flat mini-surfaces with various

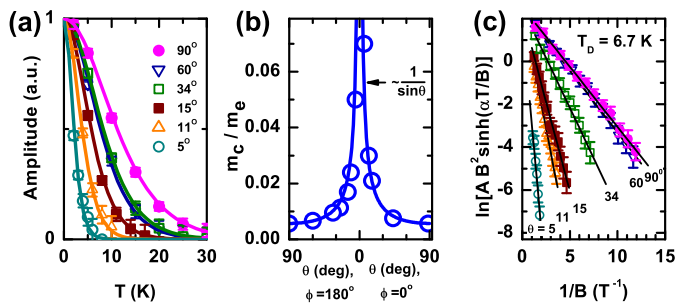


FIG. 4: (Color online) (a) Temperature dependences of the dHvA amplitudes measured at a fixed magnetic field below the quantum limit within the binary plane. Solid lines are the fits to the standard Lifshitz-Kosevich formula. (b) Angular dependence of m_c signifying the unambiguous 2D nature. (c) Dingle plots yielding the same Dingle temperature for all magnetic-field directions (A is the dHvA amplitude and $\alpha = 14.7(m_c/m_e)$ [T/K]).

orientations. Naturally, some of the mini-surfaces are perpendicular to the C_1 axis, and as long as their extent is larger than ℓ , they can produce QOs.

Let us now combine the dHvA results on $\text{Bi}_{0.91}\text{Sb}_{0.09}$ with the transport data. The bulk FS gives the total number of charge carriers, n_{bulk} , of $\sim 8.1 \times 10^{22} \text{ m}^{-3}$, which is close to the value $\sim 1.8 \times 10^{23} \text{ m}^{-3}$ estimated from R_H . This means that the observed bulk ellipsoids must be electron pockets. The band scheme [3] of $\text{Bi}_{1-x}\text{Sb}_x$ dictates that those electron pockets be located at the three L points in the BZ, which is consistent with our model to fit the data in Fig. 3(d). The surface FS is most likely a hole pocket, because the measured R_H gives an overestimated carrier concentration which is naturally understood if there is a partial cancelation of the Hall effect from the electron and hole contributions.

We note that n_{bulk} obtained from the dHvA effect is much larger than the possible concentration of impurities, donors or acceptors, of $\sim 10^{21} \text{ m}^{-3}$ (estimated from the ICP-AES analysis) in our $\text{Bi}_{0.91}\text{Sb}_{0.09}$ crystal. Then, why is the Fermi level in the bulk of $\text{Bi}_{0.91}\text{Sb}_{0.09}$ not located in the gap but goes into the conduction band, giving a rather appreciable electron concentration? We speculate that this is due to a coupling of the bulk FS to the surface FS that causes an intrinsic self-doping, but the actual mechanism is to be elucidated. Also, the amplitude of the dHvA oscillations from the 2D FS appears to be orders of magnitude larger than what is expected if each surface hole contributes a magnetic moment of $\sim \hbar e/m_c c$; this puzzle will probably be resolved if the unique properties of the surface states of a TI, the Dirac-like [25] and spin-filtered nature and the topological protection, are properly taken into account [26]. An alternative scenario that may account for the large dHvA amplitudes from the 2D FS and the unusual electron-hole coupling would be a formation of a 2D cylindrical

FS perpendicular to the bisectrix planes within the bulk BZ; however, this is probably too exotic, given the 3D crystal structure of $\text{Bi}_{1-x}\text{Sb}_x$. Clearly, there is a lot to understand about the macroscopic properties of topological insulators, and the availability of the powerful tool of quantum oscillations demonstrated here promises a vast possibility for future research.

We thank M. Hagiwara, Y. Onuki, and S.-C. Zhang for helpful discussions. This work was supported by JSPS (KAKENHI 19340078 and 2003004) and AFOSR (AOARD-08-4099).

- [1] H. Fukuyama and R. Kubo, J. Phys. Soc. Jpn **28**, 570 (1970).
- [2] P. A. Wolff, J. Phys. Chem. Solids **25**, 1057 (1964).
- [3] B. Lenoir *et al.*, J. Phys. Chem. Solids **57**, 89 (1996).
- [4] V. S. Edelman, Adv. Phys. **25**, 555 (1976).
- [5] N. B. Brandt and E. A. Svistova, J. Low Temp. Phys. **2**, 1 (1970).
- [6] K. Behnia, L. Balicas, and Y. Kopelevich, Science **317**, 1729 (2007).
- [7] L. Li *et al.*, Science **321**, 547 (2008).
- [8] L. Fu, C. L. Kane, and E. J. Mele, Phys. Rev. Lett. **98**, 106803 (2007).
- [9] L. Fu and C. L. Kane, Phys. Rev. B **76**, 045302 (2007).
- [10] J. E. Moore and L. Balents, Phys. Rev. B **75**, 121306(R) (2007).
- [11] X.-L. Qi, T. L. Hughes, and S.-C. Zhang, Phys. Rev. B **78**, 195424 (2008).
- [12] C. L. Kane and E. J. Mele, Phys. Rev. Lett. **95**, 146802 (2005).
- [13] B. A. Bernevig, T. L. Hughes, and S.-C. Zhang, Science **314**, 1757 (2006).
- [14] S. Murakami *et al.*, Phys. Rev. B. **76**, 205304 (2007).
- [15] M. König *et al.*, Science **318**, 766 (2007).
- [16] J. C. Y. Teo, L. Fu, and C. L. Kane, Phys. Rev. B. **78**, 045426 (2008).
- [17] H.-J. Zhang *et al.*, Phys. Rev. B, arXiv:0901.2762.
- [18] D. Hsieh *et al.*, Nature **452**, 970 (2008).
- [19] D. Hsieh *et al.*, Science **323**, 919 (2009).
- [20] A. Nishide, A. Taskin, Y. Takeichi, T. Okuda, A. Kakizaki, T. Hirahara, K. Nakatsuji, F. Komori, Y. Ando, and I. Matsuda, arXiv:0902.2251.
- [21] L. M. Falicov and H. Strachowiak, Phys. Rev. **147**, 505 (1966).
- [22] D. Schoenberg, *Magnetic Oscillations in Metals* (Cambridge Univ. Press, 1984).
- [23] Maximums, that are related to the crossing of the Fermi energy by Landau levels with higher occupation numbers, were chosen for this analysis to reduce contributions from frequencies other than f_1 .
- [24] The angular dependence $m_c(\phi)$ in the trigonal plane is also close to $\sim 1/\sin(90^\circ - \phi)$, but the span of ϕ is limited to $0^\circ - 30^\circ$ due to the crystal symmetry, precluding a divergence in $m_c(\phi)$.
- [25] S. G. Sharapov, V. P. Gusynin, and H. Beck, Phys. Rev. B **69**, 075104 (2004).
- [26] In magnetic fields, the Kramers degeneracy is lifted and a Zeeman gap opens in the topological surface state. But

the surface can remain metallic as long as the Fermi level is located within the surface band.